This is the accepted manuscript made available via CHORUS. The article has been published as:

Hydrodynamic flow in heavy-ion collisions with large hadronic viscosity

Chun Shen and Ulrich Heinz

Phys. Rev. C **83**, 044909 — Published 18 April 2011

DOI: 10.1103/PhysRevC.83.044909

Hydrodynamic flow in heavy-ion collisions with large hadronic viscosity

Chun Shen* and Ulrich Heinz†
Department of Physics, The Ohio State University, Columbus, OH 43210-1117, USA
(Dated: March 23, 2011)

Using the (2+1)-dimensional viscous hydrodynamic code VISH2+1 with a temperature dependent specific shear viscosity $(\eta/s)(T)$, we present a detailed study of the influence of a large hadronic shear viscosity and its corresponding relaxation time τ_π on the transverse momentum spectra and elliptic flow of hadrons produced in 200 A GeV Au+Au collisions. Although theory, in principle, predicts a well-defined relation $\tau_\pi T = \kappa(T) \times (\eta/s)\,(T)$, the precise form of $\kappa(T)$ for the matter created in relativistic heavy-ion collisions is not known. For the popular choice $\kappa = 3$ the hadron spectra are found to be insensitive to a significant rise of η/s in the hadronic stage, whereas their differential elliptic flow $v_2(p_T)$ is strongly suppressed by large hadronic viscosity. The large viscous effects on v_2 are strongly reduced if (as theoretically expected) $\kappa(T)$ is allowed to grow with decreasing temperature in the hadronic stage. This implies that, until reliable calculations of $\kappa(T)$ become available, an extraction of the hadronic shear viscosity from a comparison between VISH2+1 and a microscopic hadron cascade or experimental data requires a simultaneous fit of $(\eta/s)(T)$ and $\kappa(T)$.

PACS numbers: 25.75.-q, 25.75.Dw, 25.75.Ld, 24.10.Nz

I. INTRODUCTION

A fluid state of matter, quark-gluon plasma (QGP), is created in ultra-relativistic heavy-ion collision experiments at the Relativistic Heavy Ion Collider (RHIC) [1–4]. Theoretical analysis of these experiments established that QGP behaves like an almost perfect liquid with very small viscosity [5–7]. Much effort has been focused on determining the QGP transport parameters, in particular its specific shear viscosity $(\eta/s)_{\rm QGP}$, i.e. the ratio between its shear viscosity η and entropy density s (see [8, 9] for recent reviews).

In a recent article [10] the newly developed hybrid code VISHNU [11] has been used to extract $(\eta/s)_{\rm QGP}$ from the observed collision centrality dependence of the integrated charged hadron elliptic flow v_2. This code couples the macroscopic evolution of the QGP by the (2+1)-dimensional viscous hydrodynamic code VISH2+1 to the Boltzmann cascade UrQMD which describes the final hadronic rescattering and freeze-out stage microscopically. The microscopic simulation of the late hadronic stage is numerically costly, and a macroscopic description with viscous fluid dynamics would therefore be much preferred if valid. Unfortunately, a detailed study presented in [11] indicated that the microscopic UrQMD dynamics cannot be faithfully simulated with viscous hydrodynamics if one assumes the frequently used relationship $\tau_\pi T = 3\frac{\eta}{s}$ between the specific shear viscosity η/s and the microscopic relaxation time τ_π for the shear viscous pressure tensor $\pi^{\mu\nu}$, scaled with the temperature T of the fluid. Relations of the type $\tau_\pi T = \kappa\frac{\eta}{s}$, with constant proportionality factors κ, are found theoretically in both the extreme weak-coupling (for a massless Boltzmann gas one finds $\kappa = 6$ in Israel-Stewart theory [12, 13] and $\kappa = 5$ in the modified approach by Denicol *et al.* [14]) and extreme strong-coupling limits (where one has $\kappa = 4 - 2\ln 2 = 2.614$ for $\mathcal{N} = 4$ super-Yang-Mills theory at infinite coupling [15–17]). Other recent work, however, based on modified Kubo relations [18–21] and a deeper analysis of the Boltzmann equation and its connection to viscous hydrodynamics [14, 22, 23], suggests (in some cases strong) temperature dependence of κ.

Here we will explore one such proposed relation, $\kappa = (e+p)/p$ [19] (where e and p are the energy density and pressure of the system), which leads to a strong increase of $\kappa(T)$ with decreasing temperature in the massive hadron resonance gas below the quark confinement temperature $T_{\rm c}$. Such an increase is qualitatively consistent with certain observations made in the recent VISHNU study [11]. We here use VISH2+1 to investigate, within a purely hydrodynamic framework, systematically the consequences of increasing shear viscosity and shear pressure relaxation time in the late hadronic stage on the transverse momentum spectra and elliptic flow of soft $(p_T < 2\,{\rm GeV}/c)$ hadrons produced in Au+Au collisions at RHIC. Our work differs from an earlier study by Bożek [24] of the effects of temperature-dependent specific bulk and shear viscosities by focusing on shear viscosity and investigating situations in which the shear viscosity of the hadron gas is *larger* than that of the QGP (rather than the other way around [24]), as expected on basic theoretical grounds [25]. While the present work was being completed, a related study appeared [26] which focusses chiefly on the question whether recent data from Pb+Pb collisions at the Large Hadron Collider (LHC) [27] require an increase of the QGP shear viscosity with rising temperature.

The paper is organized as follows: In Sec. II we briefly review the viscous hydrodynamic model and discuss the specific ingredients used in the present study. The effects of a large hadronic specific shear viscosity $(\eta/s)_{\rm HG}$ on the fireball evolution are discussed in Sec. III. In

* Correspond to shen@mps.ohio-state.edu
† Email: heinz@mps.ohio-state.edu

Sec. IV we discuss the dependence of the transverse momentum spectra and elliptic flow of emitted hadrons in Au+Au collisions on $(\eta/s)_{\rm HG}$, the decoupling temperature $T_{\rm dec}$, and the collision centrality. Section V is dedicated to a detailed discussion of the viscous corrections to the freeze-out phase-space distribution and their effects on spectra and elliptic flow. All results up to this point assume a constant factor $\kappa = 3$ in the relation $\tau_\pi T = \kappa \frac{\eta}{s}$ between the specific shear viscosity η/s and the microscopic relaxation time τ_π; in Sec. VI we explore the consequences of making $\kappa(T)$ temperature dependent and letting it grow during the quark-hadron phase transition. A final discussion in Sec. VII concludes our paper.

II. VISCOUS HYDRODYNAMICS: SPECIFIC INGREDIENTS FOR THE PRESENT STUDY

`VISH2+1` [28] solves the second-order Israel-Stewart equations for causal relativistic viscous fluid dynamics [12] in the spatial plane transverse to the beam direction and in time, assuming boost-invariance of the longitudinal expansion. To avoid repetition we refer the reader interested in the technical details to earlier descriptions of the specific form of the evolution equations and the equation of state s95p-PCE used here (see specifically Sections II and III in Ref. [29]). The energy-momentum tensor is decomposed as $T^{\mu\nu} = eu^\mu u^\nu - p\Delta^{\mu\nu} + \pi^{\mu\nu}$ where $\pi^{\mu\nu}$ is the viscous pressure tensor. We consider only shear viscosity and ignore bulk viscous effects; in this situation the Israel-Stewart equations describe the evolution of $\pi^{\mu\nu}$ towards it Navier-Stokes limit $2\eta\sigma^{\mu\nu}$ on a microscopic relaxation time scale τ_π, where η is the shear viscosity and $\sigma^{\mu\nu}$ is the velocity shear tensor which evolves hydrodynamically in space and time. We initialize $\pi^{\mu\nu}$ with its Navier-Stokes value $\pi^{\mu\nu} = 2\eta\sigma_0^{\mu\nu}$ at initial time τ_0, calculated from the initial velocity profile $u^\mu = (u^\tau, u^x, u^y, u^\eta) = (1, 0, 0, 0)$.

The generation of hydrodynamic flow from the pressure gradients in the system is controlled by the fluid's equation of state (EOS) for which we use s95p-PCE [29, 30] with chemical decoupling temperature $T_{\rm chem} = 165\,$MeV. This EOS interpolates between state-of-the-art Lattice QCD data at high temperatures and a chemically frozen hadron resonance gas at low temperatures. Chemical freeze-out at $T_{\rm chem} = 165\,$MeV guarantees that the final hadron yields, calculated by integrating the final hadron momentum spectra obtained from the hydrodynamic output along an isothermal decoupling surface of temperature $T_{\rm dec} < T_{\rm chem}$ via the Cooper-Frye procedure [31] followed by resonance decay [32, 33], agree with experimental measurements in 200 $A\,$GeV Au+Au collisions at RHIC [3, 34, 35]. At decoupling, we parametrize the local distribution function in the Cooper-Frye formula by a local thermal equilibrium function plus a small viscous correction which depends on the value of the viscous pressure tensor $\pi^{\mu\nu}$ on the freeze-out surface and increases quadratically with particle momentum [29, 36]. Unless noted otherwise, we use $T_{\rm dec} = 120\,$MeV.

We initialize the hydrodynamic evolution with an energy density profile obtained from the optical `fKLN` model [37–39]. The model yields the initial gluon density distribution which, after thermalization, gives directly the initial entropy density which is then converted to energy density using the EOS s95p-PCE. The normalization of the initial entropy density is adjusted in the most central collisions to reproduce the finally measured charged hadron multiplicity. Due to viscous entropy production, changing η/s requires a readjustment of this normalization to keep the final multiplicity fixed. After normalization in central collisions, the centrality dependence of the final charged hadron multiplicity is obtained directly from the `fKLN` model, without further adjustment of parameters.

The key ingredients whose influence on the generation of radial and elliptic flow we want to study here are the temperature dependence of the specific shear viscosity η/s and of the proportionality constant between η/s and the temperature-scaled microscopic relaxation time $\tau_\pi T$, $\kappa = \frac{\tau_\pi T}{\eta/s}$. Specifically, we will explore scenarios where $\eta/s = 0.16$ is a constant in the QGP phase but increases by variable amounts during the transition from QGP to hadrons, using the following parametrization for its temperature dependence:

$$\frac{\eta}{s}(T) = \frac{(\eta/s)_{\rm QGP} + (\eta/s)_{\rm HG}}{2} + \frac{(\eta/s)_{\rm QGP} - (\eta/s)_{\rm HG}}{2} \tanh\left(40\frac{T-T_{\rm c}}{T_{\rm c}}\right). \quad (1)$$

Here $T_{\rm c} = 170\,$MeV, and $(\eta/s)_{\rm QGP} = 0.16$ and $(\eta/s)_{\rm HG}$ are (different) constants for the QGP and HG (hadron gas) phases. We will explore the range $0.16 \le (\eta/s)_{\rm HG}$

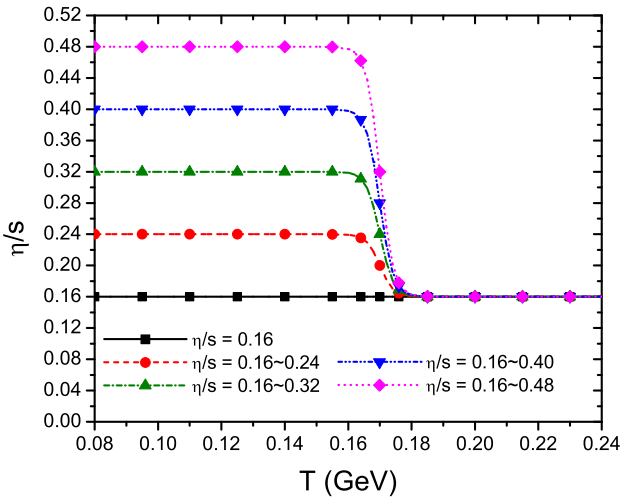

FIG. 1. (Color online) Five choices for the temperature dependent $(\eta/s)(T)$ studied in this work. The constant values at low T are multiples of $0.08 \approx \frac{1}{4\pi}$.

≤ 0.48, as illustrated in Figure 1. In the next three sections κ will be held constant at $\kappa = 3$;[50] consequences of a temperature dependent $\kappa(T) = (e+p)/p$ will be explored in Sec. VI.

III. HYDRODYNAMIC EVOLUTION

In order to study how the fireball evolves with a temperature dependent $(\eta/s)(T)$ that increases in the HG phase, we graph the time evolution for the average transverse flow velocity $\langle\langle v_\perp \rangle\rangle$ (the average over the transverse plane being defined with the lab-frame energy density $\gamma_\perp e$ as weight), the spatial eccentricity $\varepsilon_x = \frac{\langle\langle y^2 - x^2 \rangle\rangle}{\langle\langle y^2 + x^2 \rangle\rangle}$ of the lab-frame energy density distribution, the *flow* momentum anisotropy $\varepsilon_p = \frac{\langle T_0^{xx} - T_0^{yy} \rangle}{\langle T_0^{xx} + T_0^{yy} \rangle}$ (where $\langle \ldots \rangle$ denotes simple integration over the transverse plane and $T_0^{\mu\nu}$ is the ideal fluid part of the energy-momentum tensor, without viscous pressure contributions), and the *total* momentum anisotropy $\varepsilon_p' = \frac{\langle T^{xx} - T^{yy} \rangle}{\langle T^{xx} + T^{yy} \rangle}$ for different choices of the temperature dependence of η/s.

Since shear viscosity leads to viscous heating which generates entropy, holding the finally observed hadron multiplicity fixed requires that an increase in $(\eta/s)(T)$ must be accompanied by a decrease of the initial entropy of the fireball. We implement this by a decrease of the normalization of the initial entropy density distribution, keeping its shape fixed. Whereas for fixed initial conditions an overall increase of η/s leads to stronger radial acceleration due to a positive contribution from the viscous pressure tensor $\pi^{\mu\nu}$ to the transverse pressure gradients [36, 40–43], this effect is largely compensated [26, 29, 44] after rescaling the initial entropy density to ensure fixed final multiplicity. For our temperature-dependent η/s this compensation no longer works in the same way: after rescaling the initial entropy density profile, to compensate for increased viscous heating in the hadronic phase, the QGP core shrinks and the HG corona grows in size. Since the viscous pressure is relatively larger in the hadronic phase than in the QGP, the *effective* transverse pressure gradient is *reduced* when increasing η/s only in the hadronic phase, leading to weaker radial acceleration. This can be seen in Fig. 1a, where we see a reduction oof the growth rate of the average radial flow velocity $\langle\langle v_\perp \rangle\rangle$ with increasing values of $(\eta/s)_{\rm HG}$, holding $(\eta/s)_{\rm QGP} = 0.16$ fixed.

The larger shear viscosity in the hadronic corona leads to a more rapid initial decay[51] of the spatial fireball eccentricity ε_x (see Fig. 2b) and a slower growth rate and lower asymptotic value of the flow momentum anisotropy ε_p (Fig. 2c, open symbols). The spatial eccentricity curves in Fig. 2b all cross around $\tau - \tau_0 = 4.5\,{\rm fm}/c$, indicating the transition from stronger decay of ε_x at early times to weaker decay at late times for larger values of $(\eta/s)_{\rm HG}$. This is a consequence of the reduced flow anisotropy ε_p shown in Fig. 2c.

The lines with filled symbols in Figure 2c show that

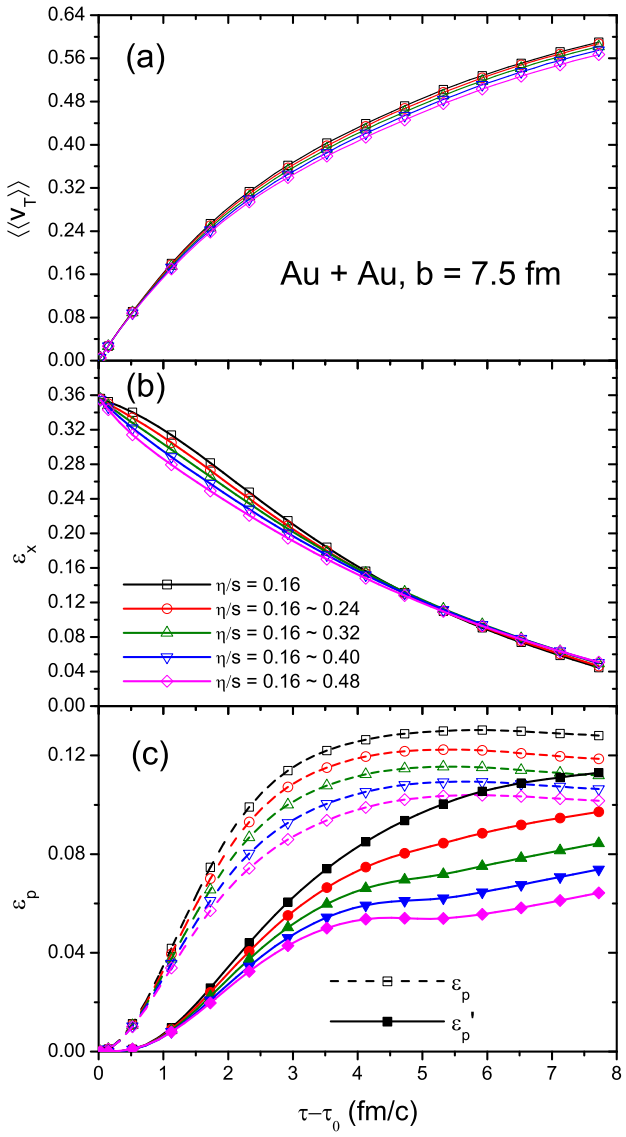

FIG. 2. (Color online) The average radial flow $\langle\langle v_\perp \rangle\rangle$, spatial eccentricity ε_x, and the flow and total momentum anisotropies ε_p and ε_p' for Au+Au collisions at $b = 7.5$ fm as functions of hydrodynamic evolution time $\tau - \tau_0$, for $\tau_0 = 0.4\,{\rm fm}/c$ and kinetic freeze-out temperature $T_{\rm dec} = 120$ MeV. Lines with different symbols correspond to different temperature dependences of η/s as shown in Fig. 1.

the effects of increased hadronic viscosity on the asymptotic values of the total momentum anisotropy ε_p' are much stronger than on the flow anisotropy ε_p: while the latter decreases by about 25% from $(\eta/s)_{\rm HG} = 0.16$ to $(\eta/s)_{\rm HG} = 0.48$, the corresponding decrease for ε_p' is almost twice as large. Also, most of the effect on ε_p' happens at late times $\tau - \tau_0 > 4.5\,{\rm fm}/c$ when most of the matter has converted into hadron gas. This reflects the growth of the Navier-Stokes value $\pi^{\mu\nu}_{\rm NS} = 2\eta\sigma^{\mu\nu}$ of the viscous pressure contribution to $T^{\mu\nu}$ in the hadronic phase where $\eta_{\rm HG}$ increases. In contrast to ε_p, the total momentum anisotropy ε_p' does not saturate at late times after

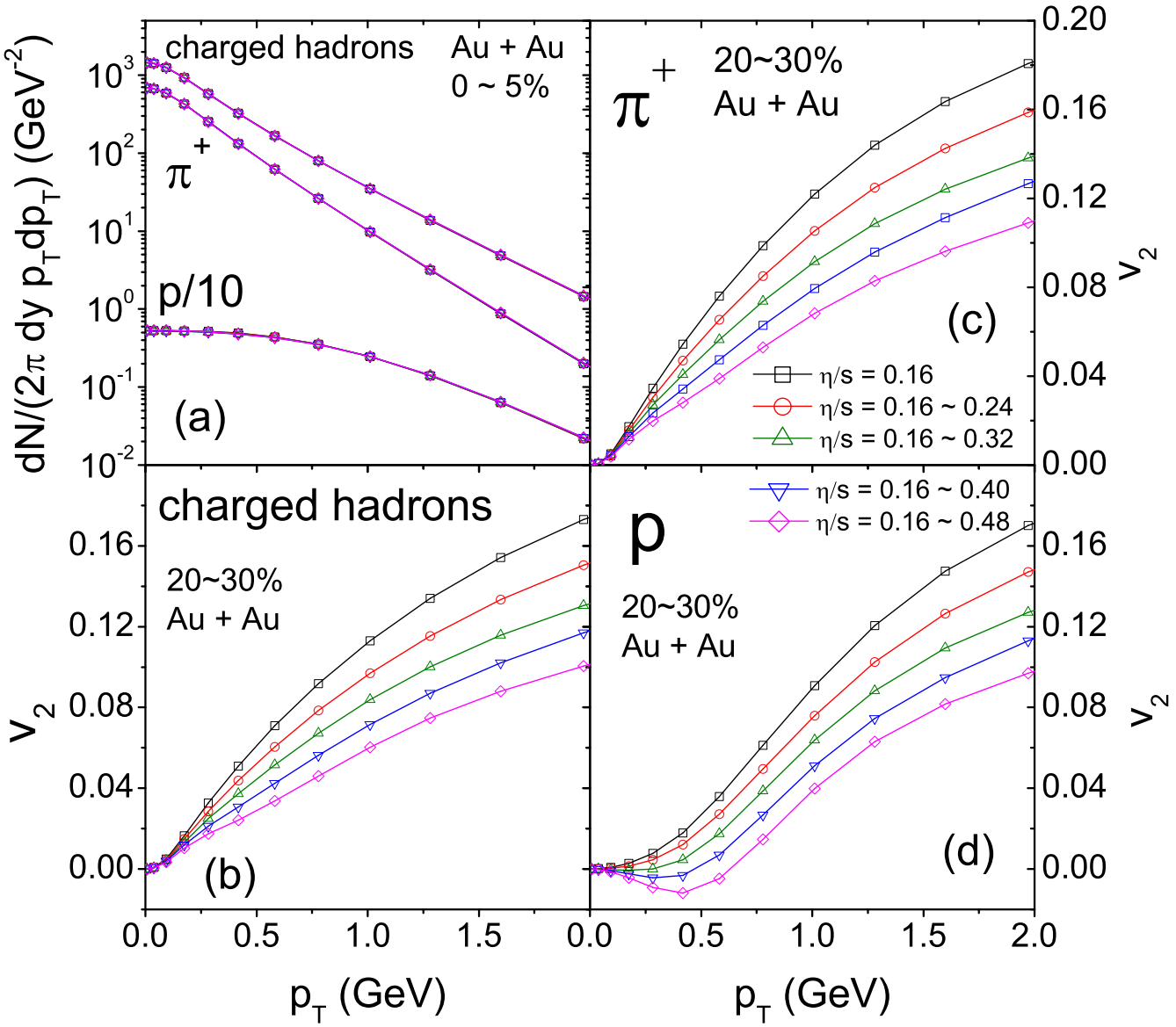

FIG. 3. (Color online) (a): Transverse momentum spectra for charged hadrons, pions, and protons from `VISH2+1` for the 5% most central Au+Au collisions ($b = 2.33$ fm). (b-c): Differential elliptic flow $v_2(p_T)$ for charged hadrons (b), pions (c) and protons (d) from Au+Au collisions at 20-30% centrality ($b = 7.49$ fm). Lines with different symbols correspond to different values of $(\eta/s)_{\rm HG}$ as shown in Fig. 1; $T_{\rm dec} = 120$ MeV. Decay products from all strong resonance decays are included. Charged hadrons include π^+, K^+, p, $\Sigma^\pm$, Ξ^-, Ω^-, and their antiparticles.

the spatial eccentricity (which drives the flow anisotropy) has essentially decayed to zero; its continued increase is due to the continuing decrease of the magnitude of the $\pi^{\mu\nu}$ components whose contribution to ε_p' is negative [43].

The large difference between the late-time values of ε_p and ε_p' for high values of $\eta_{\rm HG}$ shows that, for strong hadronic viscosity, the viscous corrections to the local thermal equilibrium distribution on the kinetic decoupling surface at $T_{\rm dec}$ are big. We will explore this in more detail in Sec. V.

IV. SPECTRA AND ELLIPTIC FLOW

A. Central and semi-peripheral Au+Au collisions

Figure 3 shows the transverse momentum spectra for charged hadrons, pions and protons from central Au+Au collisions (0−5% centrality) and their elliptic flows $v_2(p_T)$ for semiperipheral Au+Au collisions (20−30% centrality) for different choices of the hadronic shear viscosity $(\eta/s)_{\rm HG}$. The p_T-spectra in Fig. 3a are seen to be completely insensitive to the value of $(\eta/s)_{\rm HG}$. From the reduction of the radial flow seen in Fig. 2a one would

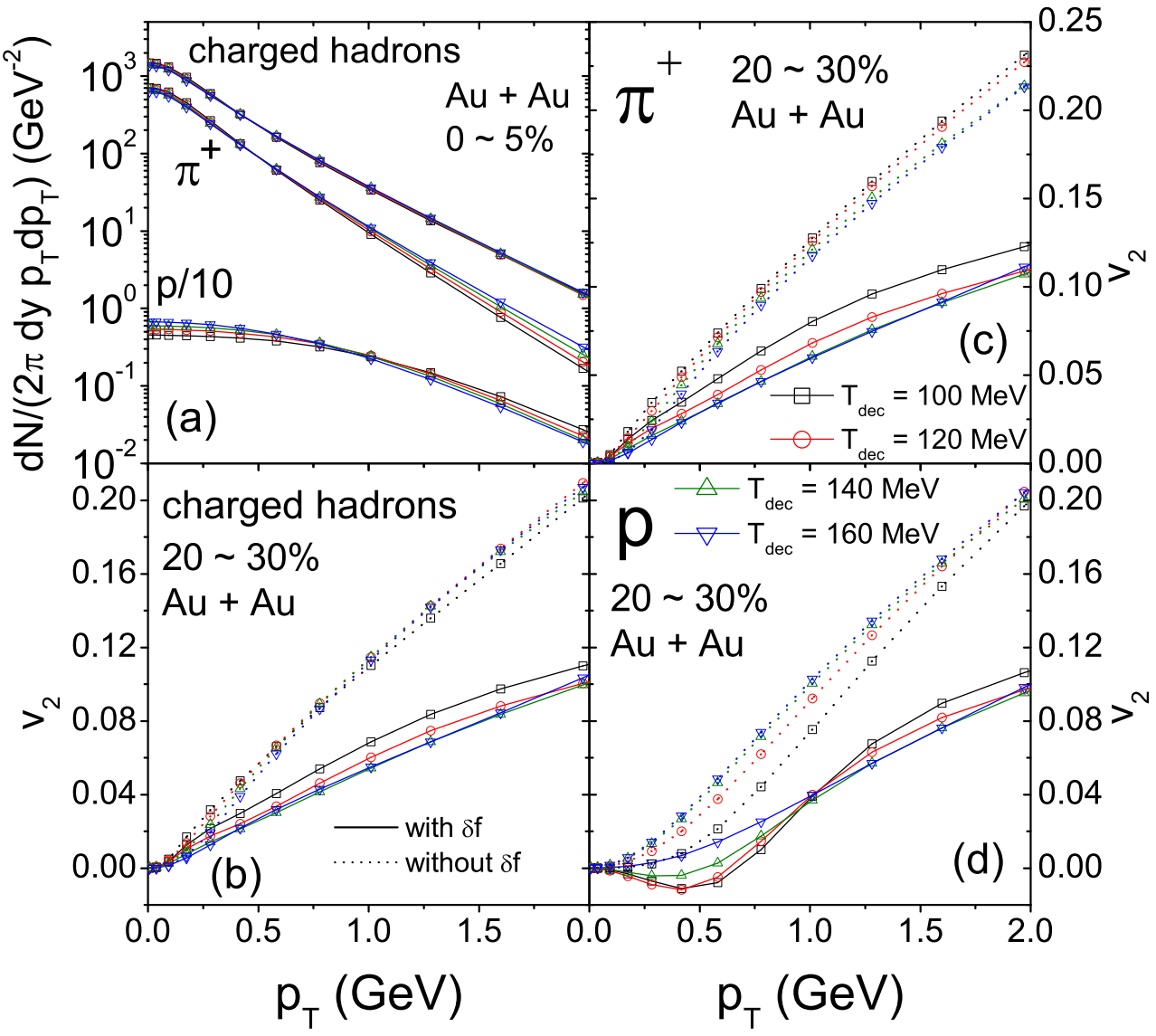

FIG. 4. (Color online) Similar to Fig. 3, for fixed $(\eta/s)_{\rm HG} = 0.48$ and different decoupling temperatures $T_{\rm dec}$ ranging from 160 to 100 MeV. In panels (b)-(d), dotted lines show $v_2(p_T)$ calculated without the δf correction whereas the solid lines show the full calculations.

have expected steeper spectra for larger $(\eta/s)_{\rm HG}$ since $T_{\rm dec} = 120$ MeV is held fixed; clearly, for $p_T < 2$ GeV/c, the viscous correction δf to the local equilibrium distribution at freeze-out (which will be analyzed in greater depth in Sec. V) happens to almost exactly compensate for the loss of radial flow, over the entire range of $(\eta/s)_{\rm HG}$ values studied here.

This is not true for the elliptic flow which is strongly reduced when the hadronic viscosity is increased (Figs. 3b-d). For protons a striking effect is seen for $(\eta/s)_{\rm HG} > 0.32$: The proton elliptic flow turns *negative* (i.e. protons show stronger flow perpendicular than parallel to the reaction plane) for low p_T. This effect is caused entirely by the δf correction. δf grows not only with p_T, as is well known, but also with the mass of the hadron. For massive hadrons, the shear viscous δf correction can be a strong effect even at $p_T = 0$. In Fig. 3 negative $v_2(p_T)$ caused by δf at low p_T is not visible for pions, but for protons and would be much stronger for Ω hyperons or J/ψ mesons [45] if they also followed viscous hydrodynamical evolution down to $T_{\rm dec} = 120$ MeV.

The effect of the δf correction is studied in Fig. 4, for various choices of the decoupling temperature $T_{\rm dec}$. We hold the hadronic shear viscosity fixed at $(\eta/s)_{\rm HG} = 0.48$, the largest value studied here. The effect of variations in $T_{\rm dec}$ on the spectra in Fig. 4a is similar to what we observed in [29]: lower decoupling temperatures cause flatter proton spectra due to larger radial flow, steeper pion spectra due to the cooling effect which dominates for light particles, and almost no change in the charged

hadron spectra whose mix of light and heavy particles effectively balances the counteracting cooling and radial flow effects.

In Figs. 4b-d we plot the differential elliptic flow for charged hadrons, pions and protons. The dotted lines show a calculation that ignores the viscous δf correction at freeze-out and thus only includes the $T_{\rm dec}$-dependence of the pure flow effects. We see that lower $T_{\rm dec}$ values suppress $v_2(p_T)$ for protons but increase it for pions at low p_T. This is really a consequence of the accompanying change of the p_T-spectra: Due to the large hadronic viscosity, very little additional flow momentum anisotropy is generated at temperatures below $T_{\rm c}$. However, due to cooling, the pion spectra get steeper with decreasing $T_{\rm dec}$, moving more of their momentum anisotropy to low transverse momenta which leads to the increase of pion $v_2(p_T)$ at low p_T. Conversely, the proton spectra get flatter, in spite of cooling, due to additional radial flow developing between $T_{\rm c}$ and $T_{\rm dec}$; consequently, their total momentum anisotropy gets shifted on average to larger transverse momenta, causing a reduction of proton $v_2(p_T)$ at low p_T (accompanied by an increase at high $p_T < 2\,{\rm GeV}/c$, beyond the range shown here). Both the flattening of the proton spectra and the shifting of their elliptic flow to larger p_T are stronger for the case of large hadronic shear viscosity ($(\eta/s)_{\rm HG} = 0.48$) studied here than for the case of temperature-independent $\eta/s = 0.16$ studied in [29]: The large hadronic viscosity generates stronger additional radial flow but less additional momentum anisotropy in the hadronic stage than does constant $\eta/s = 0.16$. Note that, without δf, proton $v_2(p_T)$ never turns negative, even for the largest hadronic shear viscosity studied in this work.

The solid lines in Figs. 4b-d show the full calculation of $v_2(p_T)$ including the δf correction. We see larger δf effects for protons than pions, due to their larger rest mass [43]. The full calculations feature a non-monotonic variation of pion and charged hadron $v_2(p_T)$ with decoupling temperature $T_{\rm dec}$: The suppression from δf is smaller for $T_{\rm dec} = 160$ MeV than for $T_{\rm dec} = 140\,{\rm MeV}$. The like explanation is that $T_{\rm dec} = 160\,{\rm MeV}$ is so close to the inflection point $T_{\rm c}$ of the shear viscosity $(\eta/s)(T)$ that, due to the finite relaxation time $\tau_\pi \sim 2\,{\rm fm}/c$ at this temperature, the viscous pressure tensor has not yet had time to fully evolve to its (larger) hadronic Navier-Stokes value whereas at $T_{\rm dec}$ complete relaxation has been achieved. At sufficiently low $T_{\rm dec}$, δf decreases with decreasing the decoupling temperature, since now η/s has reached its new, higher hadronic level and $\pi^{\mu\nu}$ becomes smaller simply due to hydrodynamic expansion [43].

B. Minimum bias collisions

In Figure 5 we show p_T spectra and differential elliptic flow for charged hadrons, pions and protons from minimum bias Au+Au collisions with $T_{\rm dec} = 120\,{\rm MeV}$. For these we summed our calculated results over all collision centralities $\leq 80\%$. The dependence on collision centrality is discussed in the next subsection.

Similar to what we saw in Fig. 3a for central Au+Au collisions, the spectra shown in Fig. 5a exhibit almost no sensitivity at all to variations of the specific shear viscosity $(\eta/s)_{\rm HG}$ in the hadron gas stage. We did observe some flattening of the charged hadron spectrum in the most peripheral (70−80%) centrality bin studied, where the viscous effects are strongest and the δf correction is largest. Due to its low weight in the average, this weak effect is not visible in the minimum bias result.

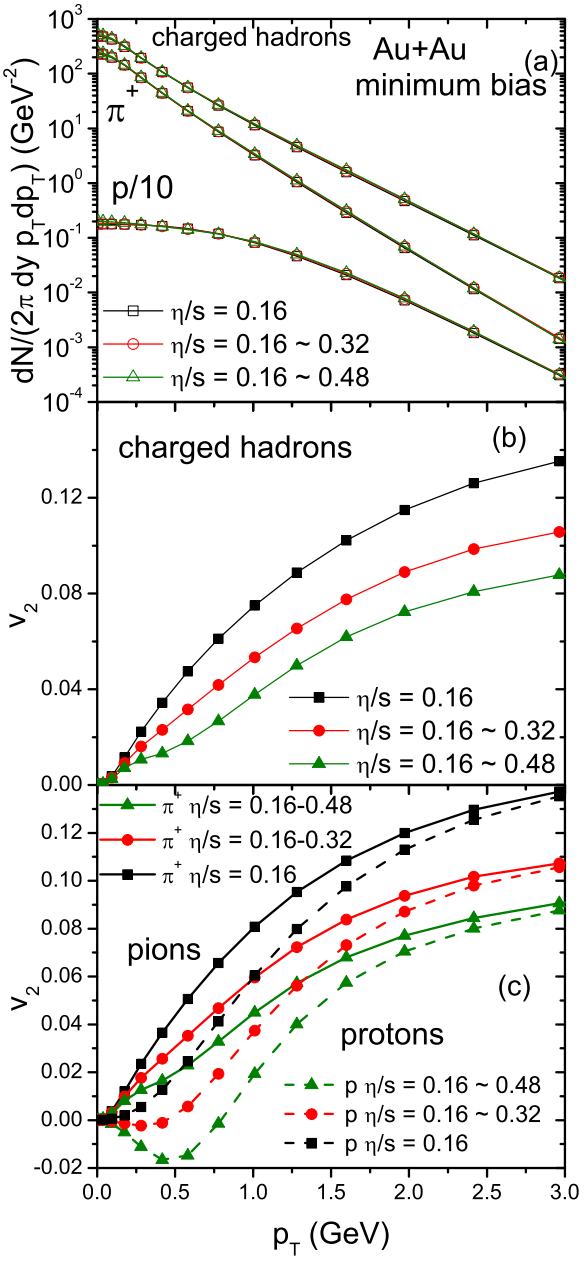

FIG. 5. (Color online) Transverse momentum spectra (a) and differential elliptic flow $v_2(p_T)$ for charged hadrons (b) and pions and protons (c) from minimum bias Au+Au collisions at RHIC, for various $(\eta/s)(T)$ as indicated (*c.f.* Fig. 1).

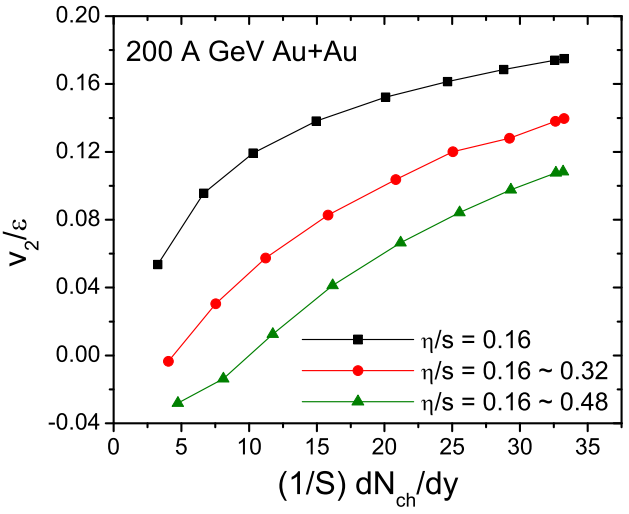

FIG. 6. (Color online) Eccentricity-scaled charged hadron elliptic flow v_2/ε as a function of the multiplicity density $(1/S)(dN_{\rm ch}/dy)$, for different values of $(\eta/s)_{HG}$. The overlap area $S=\pi\sqrt{\langle\langle x^2\rangle\rangle\langle\langle y^2\rangle\rangle}$ is calculated from the same initial profiles as the spatial eccentricity ε.

In Figures 5b and c, the minimum bias differential $v_2(p_T)$ of all charged hadrons, pions and protons are shown for different $(\eta/s)_{\rm HG}$. We see that the features observed in Fig. 3 for the specific 20−30% centrality bin carry over, qualitatively unchanged, to event samples without centrality selection: a significant increase of η/s in the hadron gas phase has a strong suppression effect on $v_2(p_T)$. However, as shown in Sec. IV A, the suppression arises mostly from the δf correction at kinetic freeze-out, with a much smaller contribution accounting for the lack of growth of the total momentum anisotropy in the hadronic phase when $(\eta/s)_{\rm HG}$ becomes large. Hence, the strong suppression of differential elliptic flow by large hadronic shear viscosity shown here is critically dependent on the validity of viscous hydrodynamics as the correct framework for evolving δf all the way down to $T_{\rm dec}=120\,$MeV. This is assumed here, but not supported by the analysis presented in [11].

C. Centrality dependence of elliptic flow

The centrality dependence of the eccentricity-scaled elliptic flow v_2/ε is shown in Fig. 6 where we graph this quantity as a function of the final charged multiplicity density $(1/S)dN_{\rm ch}/dy$. for different values of $(\eta/s)_{\rm HG}$. (We obtain v_2 by integrating $v_2(p_T)$ over all p_T, without regard to possible p_T cuts imposed by experimental constraints.) Strong suppression of v_2/ε by hadronic viscosity is observed even in the most central collisions, but the effect is stronger in peripheral collisions. An increase of $(\eta/s)_{\rm HG}$ thus not only decreases v_2/ε, but also changes the slope of its centrality dependence. We note in passing that in recent studies with the hydro+cascade hybrid code VISHNU [10] this slope was fixed and controlled by the effective dissipation encoded in the hadron cascade, and that in [11] an (unsuccessful) attempt was made to extract the temperature-dependence of $(\eta/s)_{\rm HG}$ (here assumed to be T-independent) by matching the magnitude and slope of the corresponding v_2/ε vs. $(1/S)dN_{\rm ch}/dy$ curves from VISH2+1 to those from VISHNU. We also observe that for the largest value of $(\eta/s)_{\rm HG}$ studied here, $(\eta/s)_{\rm HG}=0.48$, the total charged hadron elliptic flow turns negative in the most peripheral (70−80%) centrality bin. We found that this is caused by negative *pion* $v_2(p_T)$ around $p_T=0.5\,{\rm GeV}/c$ (i.e. close to their average p_T), caused by large δf corrections at freeze-out.[52]

V. δf CONTRIBUTIONS

Due to non-zero viscous pressure components $\pi^{\mu\nu}$, the distribution function $f_i(x,p)$ for hadron species i must deviate on the freeze-out surface from local equilibrium:

$$f_i(x,p) = f_{{\rm eq},i}(x,p) + \delta f_i(x,p). \tag{2}$$

We use [36]

$$\delta f_i = f_{{\rm eq},i}\cdot\frac{1}{2}\frac{p^\mu p^\nu}{T^2}\frac{\pi_{\mu\nu}}{e+p}, \tag{3}$$

noting that also other forms have been suggested in the literature [46, 47]. The numerator can be written as

$$\begin{aligned}
&p^\mu p^\nu \pi_{\mu\nu}(x) \\
&\quad= \pi^{\tau\tau}(x)\Big[m_T^2\big(2\cosh^2(y-\eta)-1\big)+\frac{p_T^2}{v_\perp^2}\frac{\sin(2\phi_p)}{\sin(2\phi_v)} \\
&\qquad -2\frac{p_T}{v_\perp}m_T\cosh(y-\eta)\frac{\sin(\phi_p+\phi_v)}{\sin(2\phi_v)}\Big] \\
&\quad+\Sigma(x)\Big[-m_T^2\sinh^2(y-\eta)+\frac{p_T^2}{2}\Big(1-\frac{\sin(2\phi_p)}{\sin(2\phi_v)}\Big) \\
&\qquad +p_T m_T\cosh(y-\eta)v_\perp\frac{\sin(\phi_p-\phi_v)}{\tan(2\phi_v)}\Big] \\
&\quad+\Delta(x)\Big[p_T m_T\cosh(y-\eta)v_\perp\frac{\sin(\phi_p-\phi_v)}{\sin(2\phi_v)} \\
&\qquad -\frac{p_T^2}{2}\frac{\sin(2(\phi_p-\phi_v))}{\sin(2\phi_v)}\Big]
\end{aligned} \tag{4}$$

where $\Sigma=\pi^{xx}+\pi^{yy}$, $\Delta=\pi^{xx}-\pi^{yy}$. Because of boost-invariance, tracelessness and orthogonality to u^μ, only three components of $\pi^{\mu\nu}$ are independent; we take them as Σ, Δ, and $\pi^{\tau\tau}$. $m_T=\sqrt{m^2+p_T^2}$ is the transverse mass of the particles, ϕ_p is the azimuthal angle of $\boldsymbol{p}_T$, and $\phi_v(x)$ is the azimuthal angle of the fluid velocity $\boldsymbol{v}$ at point x.

We now discuss the individual contributions from Eq. (4) to the p_T-spectra and elliptic flow, for the cases of constant $\eta/s=0.16$ (Figure 7) and temperature-dependent $(\eta/s)(T)$ (Figure 8). In panels (a-c) we show the fractional contribution $\delta N/N_{\rm eq}$ from δf to the

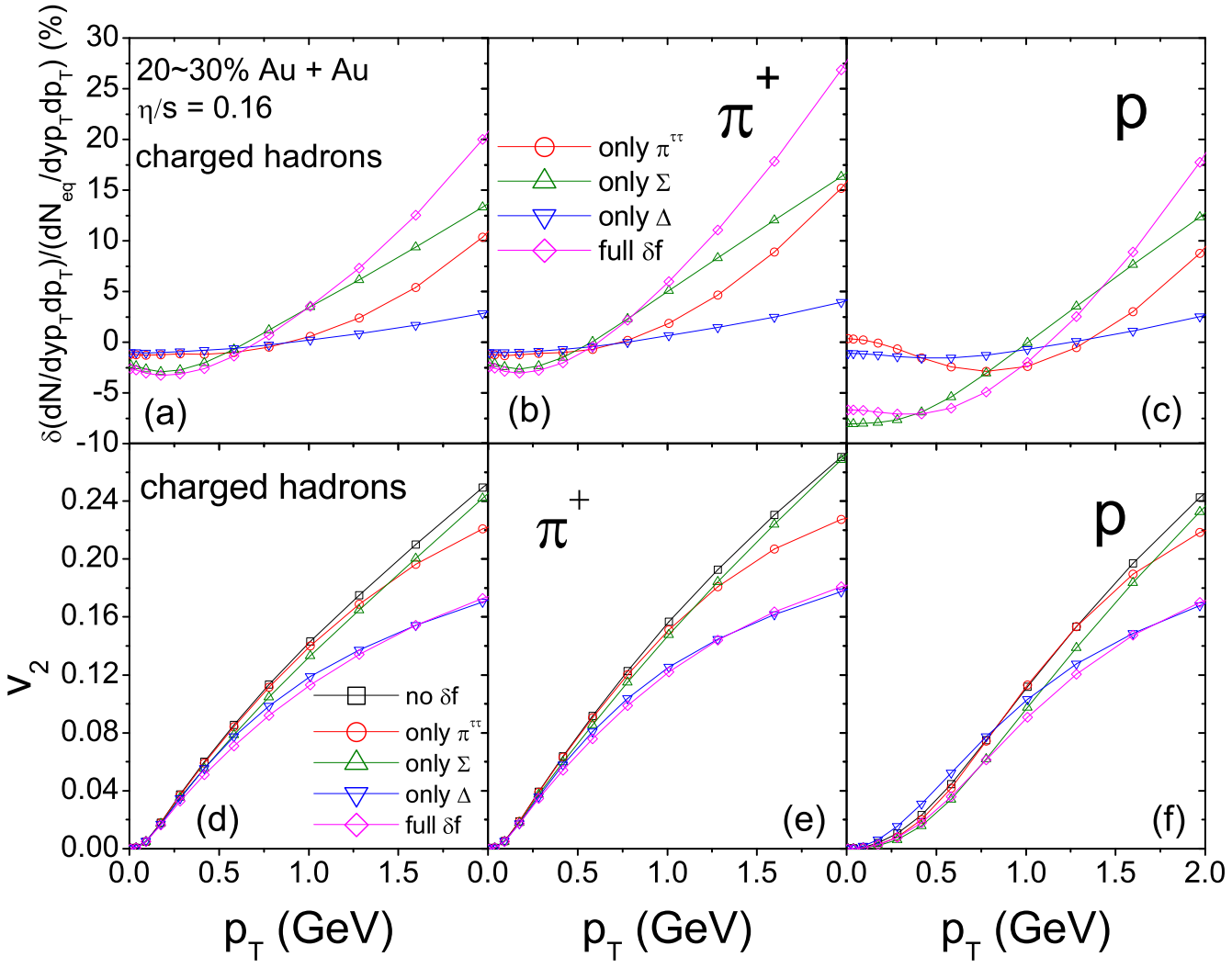

FIG. 7. (Color online) The δf correction for constant $\eta/s = 0.16$ to the p_T-spectra for charged hadrons (a), pions (b) and protons (c) at 0−5% centrality, and to their differential elliptic flow (d-f) at 20−30% centrality. Lines with different symbols denote individual contributions as described in the text.

Cooper-Frye spectra of charged hadrons (a), pions (b) and protons (c). At low p_T, the contributions proportional to $\pi^{\tau\tau}$ and Δ (first and last terms on the r.h.s. of Eq. (4)) are small and overshadowed by the contribution from the average transverse viscous pressure Σ. The first (negative) term $\sim -m_T^2$ in the expression multiplying Σ dominates at low p_T. It obviously grows with rest mass, leading to large negative $\delta N/N_{\rm eq}$ corrections at low p_T for heavy hadrons such as Ω and J/ψ [45]. For protons the effect remains below 10% in central Au+Au collisions, i.e. δf corrections are small and the calculation is reliable. At larger p_T, all three contributions in Eq. (4) turn positive and $\delta N/N_{\rm eq}$ switches sign (around 0.5 GeV/c for pions and around 1 GeV/c for protons). Again, the term $\sim\Sigma$ first dominates, but since it grows only linearly at large p_T it is eventually (at $p_T \gtrsim 2$ GeV/c) overtaken by the term $\sim\pi^{\tau\tau}$. For constant $\eta/s = 0.16$, $|\delta N/N_{\rm eq}|$ remains below 25% up to $p_T = 2$ GeV/c for all three spectra shown,[53] and the calculation is therefore reliable. For large hadronic viscosity $(\eta/s)_{\rm HG} = 0.48$ (Fig. 8) the δf corrections to the p_T-spectra are larger, in particular the term $\sim\pi^{\tau\tau}$, and $|\delta N/N_{\rm eq}|$ reaches 70−80% at $p_T = 2$ GeV/c, indicating the imminent breakdown of the viscous hydrodynamic expansion $|\delta f| \ll f_{\rm eq}$.

In the lower panels of Figs. 7 and 8 we show the δf contributions to the differential $v_2(p_T)$ for charged hadrons (d), pions (e), and protons (f), again separated into their individual contributions according to Eq. (3). We see that for low p_T all three terms in Eq. (4) contribute to the suppression of elliptic flow, but that in this case at high p_T the term proportional to the viscous pressure *anisotropy* $\Delta = \pi^{xx} - \pi^{yy}$ plays the dominant role, overshadowing the terms $\sim\Sigma$ and (except for the largest hadronic viscosities) also $\sim\pi^{\tau\tau}$. The latter grows quadratically with p_T and eventually wins over the term $\sim\Sigma$; for large hadronic viscosity (Fig. 8) it even ex-

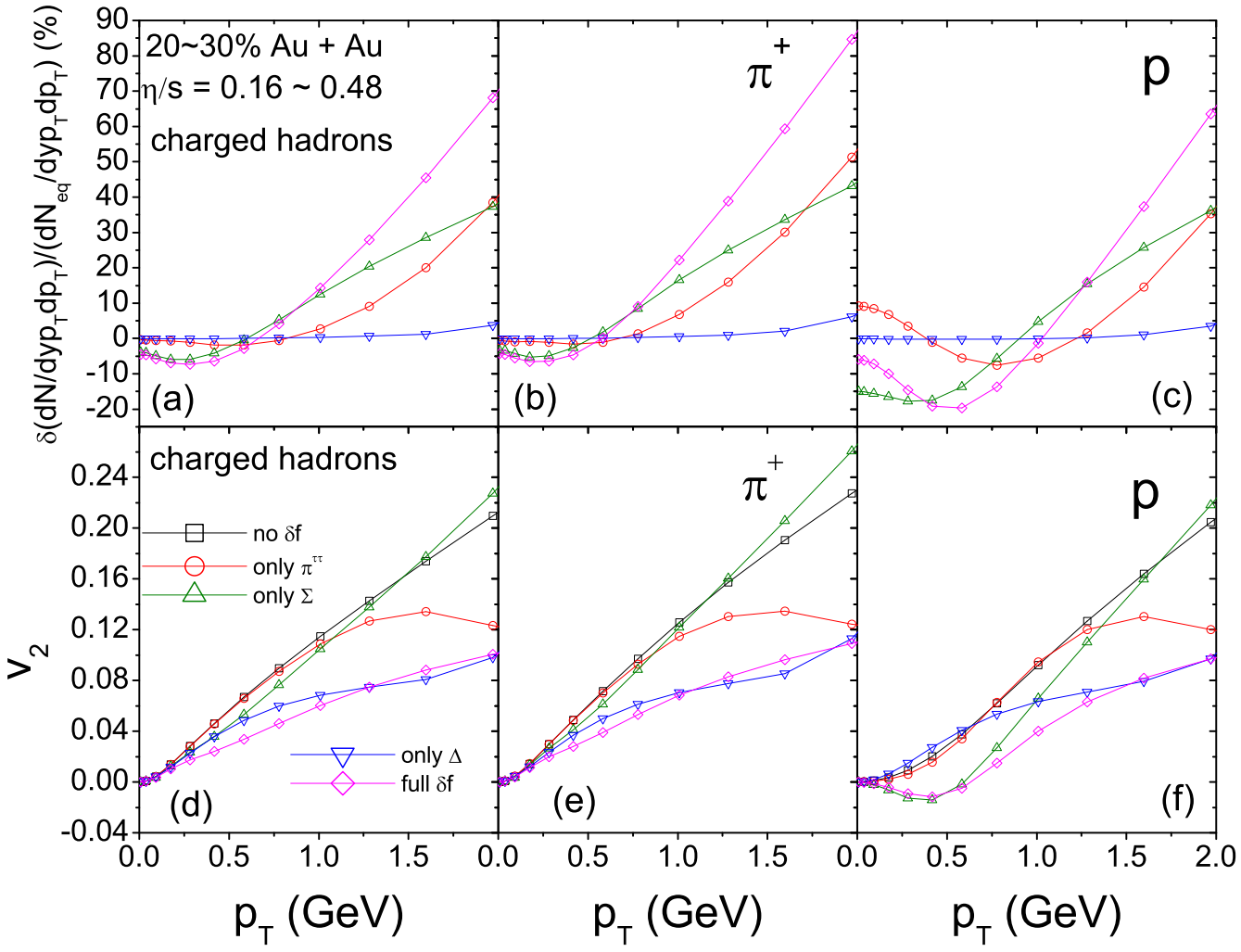

FIG. 8. (Color online) Similar to Fig. 7, but for temperature dependent $(\eta/s)(T)$, Eq. (1), with $(\eta/s)_{\rm HG}=0.48$.

ceeds the anisotropy term $\sim\Delta$ at sufficiently large p_T. The term proportional to the average transverse viscous pressure Σ individually generates a positive elliptic flow correction at large p_T (i.e. at $p_T\gtrsim 2\,{\rm GeV}/c$ for constant $\eta/s=0.16$ and at $p_T\gtrsim(1{-}1.5)\,{\rm GeV}/c$ for T-dependent $(\eta/s)(T)$ with $(\eta/s)_{\rm HG}=0.48$). Similarly the anisotropy term $\sim\Delta$ by itself increases proton elliptic flow at low p_T if the hadronic viscosity is large enough (Fig. 8f). In the sum, however, these positive individual corrections are always overwhelmed by the remaining two negative corrections, leading to an overall suppression of $v_2(p_T)$ at all p_T in all cases. Interestingly, the negative proton elliptic flow at low p_T and large $(\eta/s)_{\rm HG}$ values noted earlier (Figs. 3-5) is not caused by the viscous pressure anisotropy Δ, but by the average transverse viscous pressure Σ (green triangles in Fig. 8f). This phenomenon is driven by the effect of Σ on the proton spectra (Figs. 7c and 8c): Σ suppresses the spectra at low p_T, leading (in extreme situations) to the formation of a shoulder in the proton spectra which is known [48] to cause negative v_2.

VI. LARGE HADRONIC RELAXATION TIMES

Motivated by the study of the VISHNU model in [11] we explore in this section the consequences of very large relaxation times τ_π in the hadronic phase. Specifically, we assume a relation proposed in [19],

$$\kappa(T)=\frac{e+p}{p}(T), \tag{5}$$

which can be easily worked out for our EOS s95p-PCE and is shown in Fig. 9. In the massless limit (i.e. at large T where the EOS approaches $e=3p$), this expression approaches the value $\kappa=4$. To explore effects specifically related to the T-dependence of κ, we compare in this section results from Eq. (5) with those for constant $\kappa=4$ (and not $\kappa=3$ as in the preceding sections). The QGP viscosity is kept at $(\eta/s)_{\rm QGP}=0.16$ throughout, but we toggle $(\eta/s)_{\rm HG}$ in Eq. (1) between the two values 0.16 and 0.48 (see Fig. 1).

Figure 10 shows a similar analysis as Fig. 2, but now

comparing constant with T-dependent κ values. From Fig. 10a we conclude that the temperature dependence of κ has no visible influence on the evolution of the spatial eccentricity ε_x, irrespective of whether the specific shear viscosity η/s grows in the hadronic phase or not. On the other hand we see in Fig. 10b that a $\kappa(T)$ that grows around and below T_c as shown in Fig. 9 reduces significantly the viscous suppression of the total momentum anisotropy ε_p' that is otherwise caused by a large hadronic shear viscosity.[54] Analyzing panel (b) of Fig. 10 in more detail, we observe that during the early stage of the evolution larger hadronic relaxation times have little effect on the flow momentum anisotropy ε_p, consistent with the almost unchanged decay rate of the spatial eccentricity seen in panel (a) that drives the anisotropic flow. At late times, however, the larger $\kappa(T)$ is seen to have a small positive effect on the generation of anisotropic collective flow. Increasing the response time τ_π with which the viscous pressure tensor $\pi^{\mu\nu}$ can react to changes in the velocity shear tensor apparantly allows the collective flow anisotropy to grow more easily, with less viscous damping, than if $\pi^{\mu\nu}$ is allowed to relax to its Navier-Stokes value $\pi^{\mu\nu}_{\rm NS} = 2\eta\sigma^{\mu\nu}$ more quickly. This is a cumulative effect that becomes visible most clearly at late times when most of the fireball matter is affected by the larger $\kappa(T)$ values at lower temperatures.

The total momentum anisotropy ε_p', on the other hand, is more strongly affected by a low-temperature growth of $\kappa(T)$ (solid lines in Fig 10b). ε_p' is suppressed relative to the flow anisotropy ε_p by the non-equilibrium corrections $\sim \pi^{\mu\nu}$ in the energy-momentum tensor. When the relaxation time $\tau_\pi T$ is allowed to grow large in the hadronic phase, this suppression is found to be reduced, and the reduction is relatively larger for large values of $(\eta/s)_{\rm HG}$ (corresponding to a larger Navier-Stokes value $\pi^{\mu\nu}_{\rm NS}$) than for smaller $(\eta/s)_{\rm HG}$. We also note that this suppression

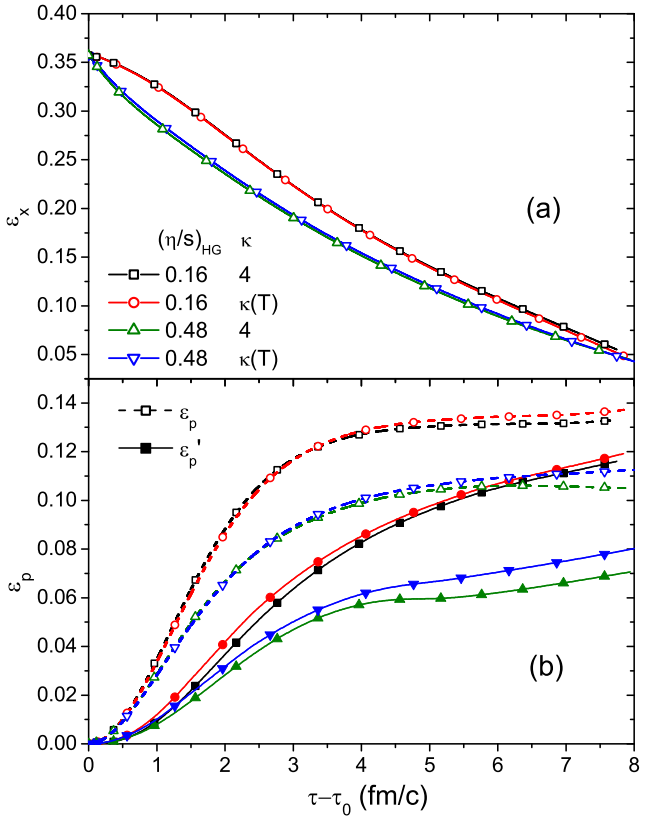

FIG. 10. (Color online) Same as Fig. 2b,c, but for $\kappa(T)$ from Eq. (5) and constant $\kappa = 4$ instead of $\kappa = 3$. For the QGP $(\eta/s)_{\rm QGP} = 0.16$ is used throughout whereas $(\eta/s)_{\rm HG}$ is varied between 0.16 and 0.48 as indicated in the legend.

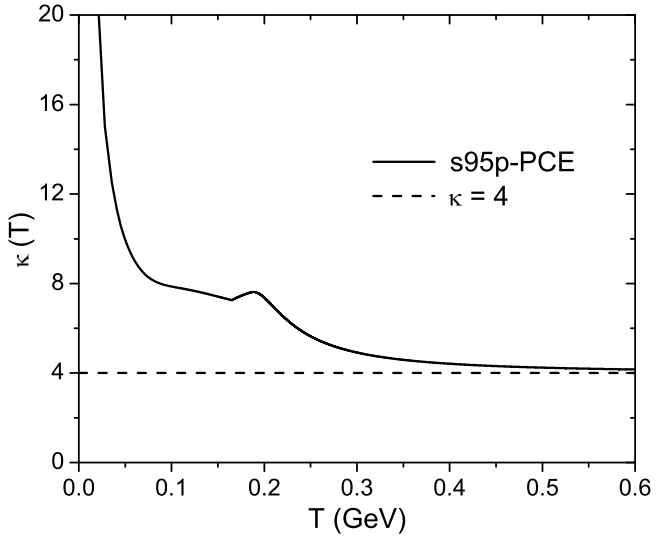

FIG. 9. The temperature dependent $\kappa(T)$ from Eq. (5) for EOS s95p-PCE (solid), compared with the massless limit $\kappa = 4$ (dashed).

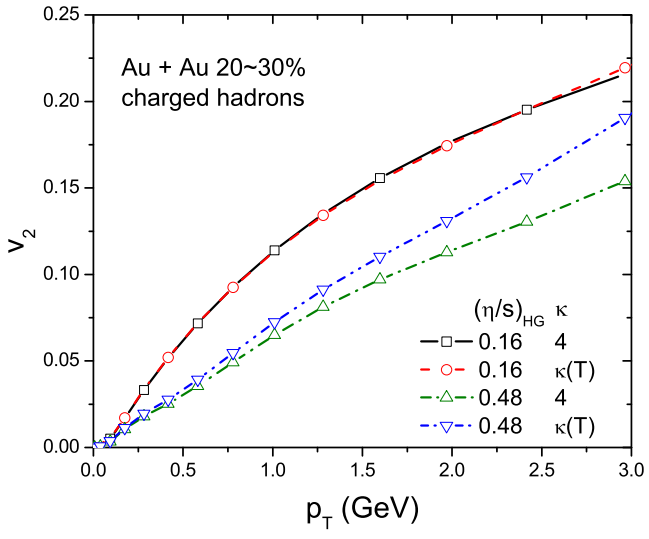

FIG. 11. (Color online) Differential elliptic flow $v_2(p_T)$ for charged hadrons, using a temperature dependent $\kappa(T)$. Same parameters as in Fig. 10.

of the $\pi^{\mu\nu}$-contribution to ε_p' is visible already at early times when the larger $\kappa(T)$ values affect only the fireball corona. In fact, for constant $\eta/s = 0.16$ (solid squares and circles) the low-temperature growth of $\kappa(T)$ leads to a bigger increase of ε_p' over ε_p at early than at late times; this is due to the larger longitudinal expansion rates at early times which lead to larger Navier-Stokes values for $\Delta = \pi^{xx} - \pi^{yy}$ everywhere, thus causing greater sensitivity to increased $\kappa(T)$ values in the fireball corona. In the case of T-dependent η/s (solid upright and inverted triangles) the effects from a delayed response τ_π are larger at late times; in this situation, the Navier-Stokes values for $\Delta = \pi^{xx} - \pi^{yy}$ grow in the hadronic phase due the sudden increase of η/s below T_c, clearly reflected by a "kink" in the growth of ε_p' around $\tau - \tau_0 = 4\,\mathrm{fm}/c$ (see upright green solid triangles in Fig 10b). This kink is largely washed out by a simultaneous rise of $\kappa(T)$ (inverted blue solid triangles in Fig 10b).

The behavior of the total momentum anisotropy ε_p' is directly reflected in the charged hadron elliptic flow, shown in Fig. 11. We point especially to the reduction of the (negative) $\pi^{\mu\nu}$ contributions to ε_p' in the case of T-dependent $(\eta/s)(T)$, which manifests itself through reduced δf corrections to $v_2(p_T)$ which again are most pronounced at large p_T (green triangles and blue inverted triangles in Fig. 11). For constant η/s, on the other hand, the larger hadronic relaxation time has little effect on the differential $v_2(p_T)$, consistent with the very small effect on the total momentum anisotropy ε_p' at late times seen in Fig. 10b.

VII. DISCUSSION AND CONCLUSIONS

Figure 11 has important implications: Comparing the blue line with inverted triangles to the case of constant κ and η/s (black squares), we conclude that the suppression of $v_2(p_T)$ reflected in the blue line could have arisen in two different ways: (i) by a large increase of η/s in the hadronic phase, accompanied by a similarly large increase of κ, as shown here, or (ii) by a much less pronounced increase of the hadronic shear viscosity, compensated by a correspondingly reduced increase of the hadronic relaxation time. In other words, the hadronic shear viscosities and relaxation times extracted from a given charged hadron $v_2(p_T)$ are strongly correlated and impossible to determine independently from a single elliptic flow measurement. Whether and how the systematic exploration of differential elliptic flow for different particle species and different collision systems at different centralities can help to resolve this ambiguity remains to be seen.

The study presented here shows that any discussion of large dissipative effects in the hadronic phase of heavy-ion collisions, reflected by specific shear viscosities and (scaled) microscopic relaxation times that grow as the system cools below the critical quark-hadron transition temperature, is really a discussion of δf, i.e. of the deviation of the freeze-out distribution function from its local equilibrium form and its reflection in the final hadron spectra and anisotropies. As the system cools and approaches kinetic freeze-out, dissipative effects become stronger and stronger, bringing the framework of viscous hydrodynamics closer and closer to breakdown. In this sense, our results have to be taken as qualitative insights but should not be confused with quantitative predictions. Their main value, as we see it, is that they shed light on and help to classify and qualitatively understand the late-stage dissipative effects on hadron spectra and their elliptic flow as seen in a realistic microscopic approach (as embodied, for example, by `VISHNU`). The results presented here do provide support to the conclusion of Ref. [11] that an effective viscous hydrodynamic description of the hadronic stage in heavy-ion collisions, if valid at all, likely requires both large shear viscosity *and* long relaxation times below T_c.

ACKNOWLEDGMENTS

`VISH2+1` was written by Huichao Song [28]. We thank Pasi Huovinen and Huichao Song for clarifying discussions, and Tomoi Koide for providing us with tables for the figures in Ref. [19] and related discussions. We also express our thanks to an anonymous referee who suggested the analyses presented in Sec. VI of this work; a preliminary version, in which we explored a much more crude and unrealistic parametrization of the temperature dependence of $\kappa(T)$ can be found on the e-print archive [49]. This work was supported by the U.S. Department of Energy under contracts DE-SC0004286 and (within the framework of the JET Collaboration) DE-SC0004104.

[1] BRAHMS Collaboration, I. Arsene *et al.*, Nucl. Phys. **A757**, 1 (2005).
[2] PHOBOS Collaboration, B. B. Back *et al.*, Nucl. Phys. **A757**, 28 (2005).
[3] STAR Collaboration, J. Adams *et al.*, Nucl. Phys. **A757**, 102 (2005).
[4] PHENIX Collaboration, K. Adcox *et al.*, Nucl. Phys. **A757**, 184 (2005).
[5] U. Heinz and P. F. Kolb, Nucl. Phys. **A702**, 269 (2002).
[6] P. F. Kolb and U. Heinz, Hydrodynamic description of ultrarelativistic heavy-ion collisions, in *Quark-Gluon Plasma 3*, edited by R. Hwa and X.-N. Wang, p. 634, World Scientific, Singapore, 2004, arXiv:nucl-th/0305084.
[7] M. Gyulassy and L. McLerran, Nucl. Phys. **A750**, 30 (2005).
[8] P. Romatschke, Int. J. Mod. Phys. **E19**, 1 (2010).
[9] U. Heinz, Early collective expansion: Relativistic hydrodynamics and the transport properties of QCD matter, in *Relativistic Heavy Ion Physics*, edited by R. Stock, Landolt-Börnstein, New Series, Vol. I 23, chap. 5-1, Springer Verlag, New York, 2010, arXiv:0901.4355.
[10] H. Song, S. A. Bass, U. Heinz, T. Hirano, and C. Shen, arXiv:1011.2783.
[11] H. Song, S. A. Bass, and U. Heinz, Phys. Rev. C **83**, 024912 (2011).
[12] W. Israel and J. M. Stewart, Ann. Phys. **118**, 341 (1979).
[13] R. Baier, P. Romatschke, and U. A. Wiedemann, Phys. Rev. C **73**, 064903 (2006).
[14] G. Denicol, T. Koide, and D. Rischke, Phys. Rev. Lett. **105**, 162501 (2010).
[15] S. Bhattacharyya, V. E. Hubeny, S. Minwalla, and M. Rangamani, JHEP **0802**, 045 (2008).
[16] R. Baier, P. Romatschke, D. T. Son, A. O. Starinets, and M. A. Stephanov, JHEP **0804**, 100 (2008).
[17] M. Natsuume and T. Okamura, Phys. Rev. D **77**, 066014 (2008).
[18] T. Koide and T. Kodama, Phys. Rev. E **78**, 051107 (2008).
[19] T. Koide, E. Nakano, and T. Kodama, Phys.Rev.Lett. **103**, 052301 (2009).
[20] G. D. Moore and K. A. Sohrabi, (2010), 1007.5333.
[21] X.-G. Huang, T. Kodama, T. Koide, and D. H. Rischke, Phys. Rev. C **83**, 024906 (2011).
[22] M. A. York and G. D. Moore, Phys.Rev. **D79**, 054011 (2009), 0811.0729.
[23] B. Betz, D. Henkel, and D. Rischke, J.Phys.G **G36**, 064029 (2009).
[24] P. Bozek, Phys. Rev. C **81**, 034909 (2010).
[25] L. P. Csernai, J. I. Kapusta, and L. D. McLerran, Phys. Rev. Lett. **97**, 152303 (2006).
[26] H. Niemi, G. S. Denicol, P. Huovinen, E. Molnar, and D. H. Rischke, arXiv:1101.2442.
[27] ALICE Collaboration, K. Aamodt *et al.*, arXiv:1011.3914.
[28] H. Song, Ph. D. Thesis, The Ohio State University (August 2009) [arXiv:0908.3656 [nucl-th]].
[29] C. Shen, U. Heinz, P. Huovinen, and H. Song, Phys. Rev. C **82**, 054904 (2010).
[30] P. Huovinen and P. Petreczky, Nucl. Phys. **A837**, 26 (2010).
[31] F. Cooper and G. Frye, Phys. Rev. D **10**, 186 (1974).
[32] J. Sollfrank, P. Koch, and U. Heinz, Phys. Lett. **B252**, 256 (1990).
[33] J. Sollfrank, P. Koch, and U. Heinz, Z. Phys. **C52**, 593 (1991).
[34] P. Braun-Munzinger, D. Magestro, K. Redlich, and J. Stachel, Phys. Lett. **B518**, 41 (2001).
[35] A. Andronic, P. Braun-Munzinger, and J. Stachel, Phys. Lett. **B673**, 142 (2009), [Erratum: Phys. Lett. B678, 516 (2009)].
[36] D. Teaney, Phys. Rev. C **68**, 034913 (2003).
[37] A. Adil, H.-J. Drescher, A. Dumitru, A. Hayashigaki, and Y. Nara, Phys. Rev. C **74**, 044905 (2006).
[38] H. J. Drescher and Y. Nara, Phys. Rev. C **75**, 034905 (2007).
[39] H.-J. Drescher, fKLN code, available at URL http://th.physik.uni-frankfurt.de/~drescher/CGC/.
[40] A. K. Chaudhuri and U. Heinz, J. Phys. Conf. Ser. **50**, 251 (2006).
[41] R. Baier and P. Romatschke, Eur. Phys. J. **C51**, 677 (2007).
[42] H. Song and U. Heinz, Phys. Lett. **B658**, 279 (2008).
[43] H. Song and U. Heinz, Phys. Rev. C **77**, 064901 (2008).
[44] P. Romatschke, Eur. Phys. J. **C52**, 203 (2007).
[45] C. Shen and U. Heinz, unpublished notes.
[46] A. Monnai and T. Hirano, Phys. Rev. C **80**, 054906 (2009).
[47] K. Dusling, G. D. Moore, and D. Teaney, Phys. Rev. C **81**, 034907 (2010).
[48] P. Huovinen, P. Kolb, U. Heinz, P. Ruuskanen, and S. Voloshin, Phys. Lett. **B503**, 58 (2001).
[49] C. Shen and U. Heinz, arXiv:1101.3703v1 (unpublished).
[50] The specific values $(\eta/s)_{\rm QGP} = 0.16$ and $\kappa = 3$ chosen here agree with those used by us in the earlier studies [10, 29] while the recent work [26] assumes $\kappa = 5$.
[51] We note that ε is defined by integrating at fixed time τ over the entire transverse plane, including both thermalized and already decoupled matter. It is possible that the strong initial decay of ε seen in Fig. 2b arises mostly from contributions in that part of the hadronic corona that has already decoupled.
[52] For 70−80% centrality and $(\eta/s)_{\rm HG} = 0.32-0.48$, we found for that for pions $v_2(p_T)$ first rises at very low p_T, then turns negative for $0.25 < p_T < 0.75\,{\rm GeV}/c$ before turning positive again and continuing to grow approximately linearly with p_T. This is different from protons whose $v_2(p_T)$ turns negative right away at small p_T, again with a minimum around $0.5\,{\rm GeV}/c$. All these effects are caused by large δf effects; in this centrality bin we do not trust viscous hydrodynamic predictions to be very robust.
[53] The δf effects on charged hadron spectra can be qualitatively understood from those on pion and proton spectra by noting that at low p_T charged hadrons are dominated by pions whereas at larger p_T heavier hadrons become increasingly more important.
[54] Please note that the extremely rapid rise of $\kappa(T)$ below $T \sim 50\,{\rm MeV}$ seen in Fig. 9 is irrelevant in this context because the fireball matter decouples already at $T_{\rm dec} = 120\,{\rm MeV}$.